Renewable Energy 150 (2020) 334–341

Contents lists available at ScienceDirect

Renewable Energy

journal homepage: www.elsevier.com/locate/renene

Direct-methane solid oxide fuel cells with an *in situ* formed Ni–Fe alloy composite catalyst layer over Ni–YSZ anodes

Xiuqing Lv [a, b], Huili Chen [a, *], Wei Zhou [c], Fangqin Cheng [d], Si-Dian Li [a], Zongping Shao [c, e]

[a] Institute of Molecular Science, Key Laboratory of Materials for Energy Conversion and Storage of Shanxi Province, Shanxi University, Taiyuan, 030006, PR China
[b] College of Chemistry and Chemical Engineering, Jinzhong University, Jinzhong, 030619, PR China
[c] State Key Laboratory of Materials-Oriented Chemical Engineering, College of Chemical Engineering, Nanjing Tech University, NO.30 Puzhu Road(S), Nanjing, 211816, PR China
[d] Institute of Resources and Environmental Engineering, Shanxi University, Taiyuan, 030006, PR China
[e] Department of Chemical Engineering, Curtin University, Perth, WA, 6845, Australia

ARTICLE INFO

Article history:
Received 4 June 2019
Received in revised form
25 December 2019
Accepted 27 December 2019
Available online 2 January 2020

Keywords:
Ni-Fe alloy composite catalyst
Ni–YSZ anode
Solid oxide fuel cells
Coking resistance
Methane based fuels

ABSTRACT

Coking on Ni surfaces limits the direct application of methane-based fuels in SOFCs with Ni-cermet anodes. Loading an anodic catalytic layer with a high catalytic activity for CH_4 conversion can effectively protect the Ni-based anode from coking and increase the cell durability. In this work, a Ni–Fe alloy composite catalyst was prepared by reducing perovskite $La_{0.7}Sr_{0.3}Fe_{0.8}Ni_{0.2}O_{3-\delta}$ (LSFN) and then evaluating its catalytic activity in the partial oxidation of CH_4. The catalyst was applied on a conventional Ni–8 mol.% Y-stabilized ZrO_2 (YSZ) anode for methane SOFCs using two methane-containing fuels (97% CH_4 –3% H_2O and 30% CH_4–70% air). The catalyst-modified cells showed much higher performances and durability than the conventional cell using a Ni–YSZ anode, indicating the potential application for direct-methane SOFCs.

1. Introduction

Solid oxide fuel cells (SOFCs) are electrochemical devices that efficiently convert the chemical energy of fuels into electrical power with low emissions [1–4]. One of the outstanding advantages of SOFCs is their ability to theoretically operate using any combustible fuel, such as H_2, syngas, solid carbon, natural gas, and hydrocarbons, etc [5–11]. The anode where fuel is electro-oxidized is one of the most important components of SOFCs. Ni cermet anodes have been widely used in SOFCs because of their excellent electronic conductivity, sufficient ionic conductivity, high catalytic performance in fuel electro-oxidation, and good compatibility with popular electrolytes. However, when methane-containing fuels are directly used, coking occurs on the Ni-based anode because Ni can catalytically break C–H bonds, which rapidly deteriorates the performance and durability of SOFCs [12–15]. Therefore, suppressing carbon deposition on the anode is important in SOFCs applications where methane-based fuels are used. Several approaches have been applied to increase the coking resistance of Ni-based anodes, such as using non-nickel-based anodes [16,17], alloying Ni with a second metal [18], doping ceria materials, and modifying the Ni surface [19]. However, all of these modifications decrease the activity of Ni cermet anodes.

Loading a catalytic layer with high catalytic activity for methane conversion over a Ni-cermet anode has been proved to suppress carbon deposition on the anode. The catalytic layer converts methane into species less prone to coking and also acts as a barrier layer to prevent the direct contact of fuel gas with the anode surface [20–23]. Ru–CeO_2 was first introduced as an anodic catalytic layer to increase the stability of SOFCs by converting hydrocarbons into syngas [24], but noble metals are too expensive to be widely applied. Non-noble metal Ni has high catalytic activity for methane reforming and cracking, which leads to coking on the Ni catalyst. Alloying Ni with other metals, such as Cu, Fe, Sn, Co, and Mo, can decrease methane cracking by reforming methane into syngas, which helps decrease coking on Ni-based catalysts. Alloys are typically doped with oxide supports to inhibit the growth of Ni particles [18,25–29]. However, the preparation method of alloy

* Corresponding author.
E-mail address: huilichen@sxu.edu.cn (H. Chen).

https://doi.org/10.1016/j.renene.2019.12.126
0960-1481/

catalysts has a significant influence on their coking resistance. Traditional preparation methods include time-consuming physical mixing [30,31] and infiltration [32,33], which often require expensive precursors. It is difficult to accurately control the grain size to obtain a uniform distribution of alloy nanoparticles, which are often closely packed and easily aggregate at high temperatures. This reduces the catalytic activity due to coking or agglomeration of the nanoparticles [34]. Thus, an easy preparation method that can ensure the uniform distribution of alloy nanoparticles on the surface of a support has been a focused of recent research. Exsolution of endogenous alloy nanoparticles from perovskite precursors via *in situ* reduction is regarded as a time-saving and effective strategy [35–37]. In this method, active metal elements are first combined into a host lattice during material synthesis, and then alloy nanoparticles exsolute from the backbone to uniformly anchor to the oxide substrate under a reducing atmosphere [38,39]. The strong interaction between the alloy nanoparticles and the oxide substrate further suppresses the aggregation of the active species.

In this work, perovskite $La_{0.7}Sr_{0.3}Fe_{0.8}Ni_{0.2}O_{3-\delta}$ (LSFN) was prepared and spray-coated over a NiO–8 mol.% Y-stabilized ZrO_2 (YSZ) anode as the catalyst layer. Under a reducing atmosphere, LSFN decomposed into $Fe_{0.64}Ni_{0.36}$, $SrLaFeO_4$, and La_2O_3 with the *in situ* exsolved FeNi alloy uniformly anchored on the oxide backbone. The catalytic activity of the alloy composite for the partial oxidation of methane (POM) was tested, and the electrochemical performance and discharge stability of the catalyst-modified SOFCs were investigated using methane based-fuels.

2. Experimental

2.1. Powder preparation

Perovskite $La_{0.7}Sr_{0.3}Fe_{0.8}Ni_{0.2}O_{3-\delta}$ (LSFN) was synthesized by a sol-gel method in which $La(NO_3)_3\cdot 6H_2O$, $Ni(NO_3)_2\cdot 6H_2O$, $Sr(NO_3)_2$ and $Fe(NO_3)_3\cdot 9H_2O$ were first dissolved in distilled water. Then, complex reagents EDTA and citric acid (CA) were sequentially added into the solution in a mole ratio of total metal ions: EDTA: CA of 1 : 1: 2. The pH of the solution was adjusted to 6–7 using aqueous ammonia. The solution was heated at 80 °C until a viscous gel formed, which was pre-treated at 250 °C for 5 h and then calcined at 950 °C for 3 h under an air atmosphere to obtain LSFN powders. The sintered LSFN sample was reduced at 800 °C for 0.5 h in a pure H_2 atmosphere.

2.2. Cell fabrication

NiO and YSZ were purchased from Chengdu Shudu Nanomaterials Technology Development Co., Ltd, and the $La_{0.8}Sr_{0.2}MnO_{3-\delta}$ (LSM) cathode was provided by the Ningbo Institute of Industrial Technology.

An anode-supported cell with a configuration of NiO-YSZ|YSZ|LSM-YSZ was fabricated by the following procedure:

First, NiO, YSZ and polyvinyl butyral (PVB) with a weight ratio of 60 : 40: 10 in ethanol were ball-milled at 300 rpm for 1 h. After drying, 0.40 g anode powder was pressed for 60 s under 120 MPa using a 15 mm diameter steel mould. Next, 0.025 g of YSZ electrolyte powders were homogenously spread on the anode layer and pressed for 90 s at 240 MPa to form a green dual-layered half-cell. The half-cell was then treated at 1400 °C for 5 h to densify the YSZ electrolyte. The cathode slurry was prepared by ball-milling LSM and YSZ powders in a weight ratio of 7:3 for 1 h with proper amounts of isopropyl alcohol, ethylene glycol and glycerol as additives. Then, the cathode slurry was sprayed on the dense YSZ electrolyte layer which had an effective area of 0.478 cm^2. This was followed by calcining in air for 2 h at 1100 °C and then covering the cathode layer by the diluted silver paste for current collection. Silver wires were fixed on the anode and cathode surfaces using silver paste to conduct current. Afterwards, the single cell was fixed onto the top of a quartz tube using silver paste.

The catalyst slurry was prepared by ball-milling a mixture of the LSFN powder and proper amounts of glycerol and isopropyl alcohol at a speed of 300 rpm for 1 h. The slurry was painted on the surface of the NiO–YSZ anode, where silver wire was attached to it, following by calcining at 800 °C for 1 h.

2.3. Characterization techniques

The crystalline structures of the as-sintered and the reduced LSFN powders were analyzed by X-ray diffraction (XRD, Rigaku D/Max-RB) using Cu $K\alpha$ radiation to collect data in the 2θ range between 20° and 80° at room temperature. Microstructures were investigated by a field emission scanning electron microscope (FESEM, JSM-7001F, JEOL) coupled with energy dispersive X-ray spectroscopy (EDX) (Bruker). Particle sizes were calculated using the Debye–Scherrer equation.

2.4. Catalytic activity tests

The catalytic activity of the reduced LSFN for POM was studied in a fixed-bed quartz-tube reactor with an ~8 mm inner diameter. About 0.2 g LSFN in the size range from 250 to 380 μm and 0.4 g SiO_2 were mixed and put in the center of the reactor for catalytic activity tests at 500–900 °C. After treating the LSFN in H_2 for 0.5 h at 800 °C, a mixed gas of CH_4–air (V:V, 3:7) was fed into the reactor from the top with a total flow rate of 30 ml min^{-1}. The effluent gases from the bottom of the reactor entered an Agilent 7820 gas chromatograph for compositional analysis. A blank experiment without catalyst was also studied for comparison under the same conditions. The values of CH_4 conversion, CO selectivity and H_2 selectivity were calculated according to the following equations:

$$\text{CO selectivity}\ (\%) = \frac{C_{CO}}{C_{CO}+C_{CO_2}}\times 100\% \quad (1)$$

$$\text{H}_2\ \text{selectivity}\ (\%) = \frac{C_{H_2}}{2(C_{CO}+C_{CO_2})}\times 100\% \quad (2)$$

$$\text{CH}_4\ \text{conversion}\ (\%) = \frac{C_{CO}+C_{CO_2}}{C_{CH_4}+C_{CO}+C_{CO_2}}\times 100\% \quad (3)$$

2.5. Performance of the cells

The electrochemical performances of single cells were tested in a 4-probe mode using an electrochemical workstation (Ivium Technologies B.V., Netherlands). The cells were sealed onto the top of a quartz tube with the anode exposed to fuel and the cathode exposed to the ambient air. The assembled cells were placed in a vertical furnace. Before testing, H_2 was used to reduce the NiO particles *in situ* in the anode and catalyst layer at 800 °C for 0.5 h. The performances were tested after the open circuit voltage (OCV) was stable.

During electrochemical measurements, the flow rate of the hydrogen, CH_4–air or CH_4–H_2O gas mixture was 80 ml min^{-1} (STP) for current-voltage (I–V) and electrochemical impedance spectroscopy (EIS) tests. Durability tests were carried out with a constant current load of 335 mA cm^{-2} at a flow rate of 15 ml min^{-1}

(STP). The EIS of the single cells were recorded under OCV conditions from 1 MHz to 0.1 Hz with a 10 mV signal amplitude.

3. Results and discussion

3.1. Structure and morphology of the cell with a catalyst layer

A schematic of an anode-supported cell test setup is shown in Fig. 1a where the catalyst layer is directly painted on the anode surface. Silver wire was adhered to the anode surface but not the catalyst surface, so that the electrical conductivity of the Ni-cermet anode wasn't influenced by the insulated catalyst layer. Fig. 1b show the cross-sectional microstructures of the membrane electrode assembly (Anode-Electrolyte-Cathode) and the catalyst layer, respectively. The thickness of both the densified electrolyte layer and the catalyst layer was about 30 μm. The anode and cathode layers were porous with the porosities of 30.20% and 21.4%, respectively, and adhered well to the YSZ electrolyte, to ensure a low ohmic resistance and efficient charge transfer at the interface. The catalyst layer adhered to the anode layer as well.

3.2. Structural characterization of as-sintered and reduced LSFN powders

The structure of as-sintered LSFN showed a typical perovskite-type oxide (ICSD: 82-1964) in the XRD spectra in Fig. 2a. The average LSFN particle size was 26.32 nm, as calculated from the 2θ diffraction peaks of 32.80°, 46.95° and 58.25°. After being treated in a reducing atmosphere at 800 °C for 0.5 h, the perovskite phase of LSFN completely decomposed (Fig. 2b), and a composite of a K_2NiF_4-type oxide $SrLaFeO_4$ (ICSD: 71-1744), La_2O_3 (ICSD: 83-1344) and $Fe_{0.64}Ni_{0.36}$ (ICSD: 47-1405) alloy formed. The particle size of $Fe_{0.64}Ni_{0.36}$ was calculated from the diffraction peaks at 2θ angles of 43.47° and 50.94°. The particle size of $SrLaFeO_4$ was calculated from the diffraction peaks at 2θ angles of 31.18°, 32.54° and 46.68°. The particle size of La_2O_3 was calculated based on the diffraction peaks at 2θ angles of 26.01°, 30.00° and 46.01°. The average particle sizes of $Fe_{0.64}Ni_{0.36}$, $SrLaFeO_4$ and La_2O_3 are ca. 19.66 nm, 37.66 nm and 8.64 nm, respectively.

$SrLaFeO_4$ with exsolved alloy particles has been reported to be a component of some composite anodes for hydrocarbon fuels [40,41]. Xu et al. demonstrated that $SrLaFeO_4$ was a promising

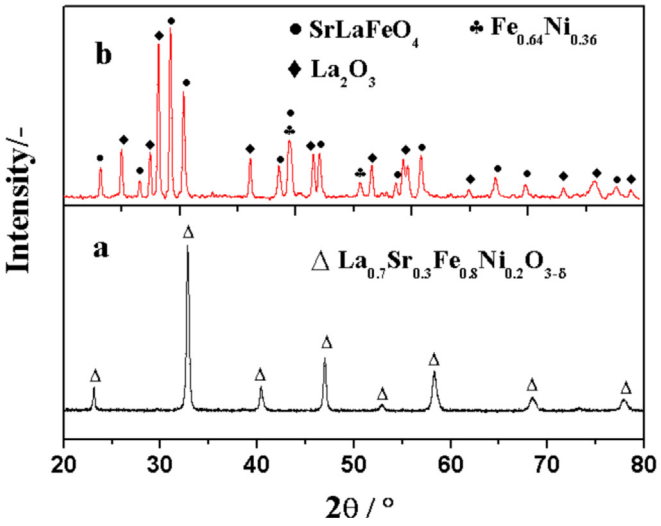

Fig. 2. XRD patterns of a) as-prepared LSFN and b) reduced LSFN.

candidate for an SOFC anode due to its good electrocatalytic activity, high stability under a reducing atmosphere and resistance to coking and sulfur [42]. La_2O_3 was also shown to be a good activator to improve the operational stability and coking resistance on Ni-based anodes to hydrocarbons [43]. Therefore, it is expected that the reduction products, $SrLaFeO_4$, La_2O_3 and $Fe_{0.64}Ni_{0.36}$ will have good catalytic performance in the POM reaction.

3.3. Catalytic activity of the reduced LSFN for POM reaction

The catalytic activity of LSFN in the POM was compared with a control experiment without any catalyst in fixed-bed reactors from 500 to 900 °C. A mixture of CH_4–air (V:V, 3:7) was used, with a CH_4 to O_2 ratio close to the stoichiometric ratio of CH_4 partial oxidation. As shown in Fig. 3a, the CH_4 conversion increased with the temperature both with and without catalyst. At 900 °C, the CH_4 conversion over the reduced LSFN catalyst reached 98.24%, which was nearly 2.7 times higher than that without catalyst (36.83%). Below 750 °C, the CH_4 conversion efficiency was nearly zero in the absence of catalyst, while it reached up to 22.48% at 500 °C with the

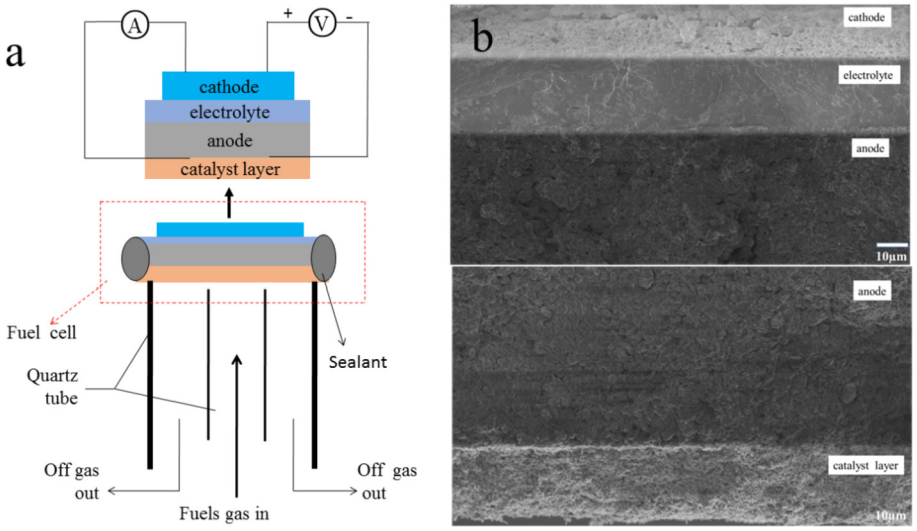

Fig. 1. a) Schematic of the fuel cell test setup and b) cross-sectional SEM image of a cell and catalyst layer.

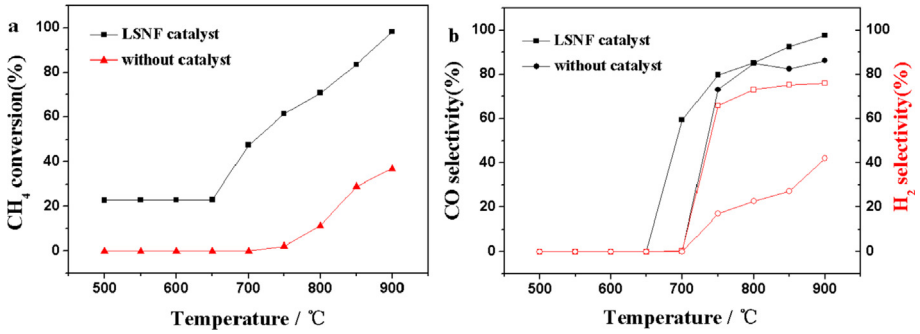

Fig. 3. a) CH_4 conversion and b) CO and H_2 selectivity with and without the *in-situ* reduced LSFN catalyst in a CH_4–air (V:V, 3:7) atmosphere in the range of 500–900 °C.

reduced LSFN catalyst. The conversion did not change as the temperature increased from 500 to 650 °C because the catalytic activity of LSFN was low below 650 °C.

As shown in Fig. 3b, the CO and H_2 selectivity for the reaction over the reduced LSFN were 97.62% and 75.94% at 900 °C, which significantly exceeded that of the blank (86.25% and 42.12%). This result indicated that the Ni–Fe alloy composite catalyst had a high activity in the POM reaction.

In our previous work [40], the catalytic activity of reduced $La_{0.8}Sr_{0.2}Co_{0.4}Fe_{0.6}O_3$ (LSCF) in the POM was studied using 50% CH_4–50% O_2 with an O/C ratio of 2, in a rich oxygen atmosphere. The CH_4 conversion efficiency was only 88% at 950 °C with a CO selectivity of 69%. In this work, the O/C ratio of fuel was 0.98, with a lower oxygen content, but a higher CH_4 conversion. Compared with the reduced LSCF, the reduced LSFN showed a higher catalytic activity towards the POM. The relatively high CH_4 conversion in a low-oxygen atmosphere reveals that the composite catalyst layer may function as an excellent anodic catalyst for SOFCs.

3.4. Electrochemical performance of cells fed with CH_4-based fuels

The catalytic activity tests indicated that the composite alloy catalyst had an excellent catalytic activity for the POM reaction. Loading the catalyst onto a Ni-YSZ anode would likely improve the coking resistance when methane-based fuels are applied because CH_4 would be converted into syngas which can be further electrochemically oxidized at the three-phase-interface of the anode layer.

An anode-supported cell using LSFN as the anodic catalyst layer was used to study the coking resistance of a Ni-YSZ anode. The electrochemical performances of the catalyst-modified cells were tested when CH_4–H_2O (3% H_2O) and CH_4–air (V:V, 3:7) fuels were used, designated as (LSFN/Ni–YSZ)–(CH_4–H_2O) and (LSFN/Ni–YSZ)–(CH_4–air), respectively. For comparison, the conventional cells without the catalyst layer were also prepared and designated as (Ni–YSZ)–(CH_4–H_2O) and (Ni–YSZ)–(CH_4–air), respectively.

The I–V(P) curves of (Ni–YSZ)–(CH_4–H_2O) in Fig. 4a show peak power densities (PPDs) at 850, 800, and 750 °C of 0.546, 0.343 and 0.199 W cm^{-2}, respectively. (LSFN/Ni–YSZ)–(CH_4–H_2O) demonstrated PPDs of 0.688, 0.421 and 0.242 W cm^{-2} (Fig. 4b) at the respective corresponding temperatures. The catalyst-modified cell showed a 26.01% increase in the PPD at 850 °C compared with the conventional cell. When the fuel was switched from CH_4–H_2O to CH_4–air, both the OCVs and performances decreased. The drop of OCVs was attributed to an increase in the oxygen pressure in the anode because of the presence of air in the fuel, which lowered the methane concentration and decreased the cell performance. For (LSFN/Ni–YSZ)–(CH_4–air), the PPDs at 850, 800 and 750 °C were 0.539, 0.356 and 0.237 W cm^{-2}, respectively, while for (Ni–YSZ)–(CH_4–air), the PPDs were 0.433, 0.303 and 0.188 W cm^{-2} at the respective corresponding temperatures. Compared with Ni–YSZ, LSFN/Ni–YSZ showed a ~24.48% increase in the PPD at 850 °C (Fig. 5). These results indicate that loading a catalyst layer on the Ni-YSZ anode increased the cell performances. Since the cell materials and fabrication process were identical except for the composite catalyst layer, the improvement in the cell performance was likely due to a lower polarization loss in the anode. In this work, the concentration of H_2 and CO in the fuel increase due to the CH_4 conversion by the catalyst layer since 1 mol CH_4 can produce 2 mol H_2 and 1 mol CO. This not only has a low polarization resistance for the electrochemical reaction, but also supplies fuel to generate power [44–46]. Therefore, the anodic catalyst layer plays an important role in reducing the coking on the Ni–YSZ anode and also improving the electrochemical performances.

The electrochemical impedance spectroscopy (EIS) provides the ohmic resistance (R_o) and polarization resistance (R_p). The real-axis intercept at high frequencies represents the R_o due to the electrolyte, electrodes and lead wires, which is greatly dependent on temperature when the same electrolyte is used. The difference between the high and low-frequency intercepts with the real axis is the R_p value, which is associated with electrochemical reactions and mass transfer processes. Fig. 6 and Fig. 7 show the EIS spectra of LSFN/Ni–YSZ and Ni–YSZ at 850 °C fed with CH_4–H_2O fuel and CH_4–air fuel, respectively, which shows that the entire resistance of the cell depends on R_p. In Fig. 6a, nearly identical R_o values were obtained for Ni–YSZ (0.105 Ω cm^2) and LSFN/Ni–YSZ (0.108 Ω cm^2). The catalyst-modified cell showed a smaller R_p than that without the catalyst layer, especially at the low frequencies, which implies that the gas diffusion is promoted. The Bode plot in Fig. 6b shows that the catalyst-modified cell has lower impedances in the entire frequency domains than the conventional cell. This indicates that both the mass and charge transfers were accelerated after the catalyst layer was loaded onto the Ni-YSZ anode. The Ni–YSZ and LSFN/Ni–YSZ Bode plots exhibit peaks at about 11 Hz and 18 Hz, respectively, indicating a mass transfer electrode process. When using CH_4–air fuel, the EIS of LSFN/Ni–YSZ and Ni–YSZ show a similar trend with those using CH_4–H_2O fuel (Fig. 7) but larger R_p values because of the lower fuel concentration due to the dilution by N_2.

3.5. Durability tests at constant current density

As shown in Fig. 8, when fed with CH_4–H_2O and CH_4–air, the voltage changes of LSFN/Ni–YSZ with time were monitored at a constant current density of 335 mA cm^{-2} at 800 °C. For comparison, the same profiles for Ni–YSZ were also tested. The voltage of Ni–YSZ dropped to zero after feeding CH_4–H_2O for ~17 min and CH_4–air for ~10 h. The rapid voltage drop was potentially caused by

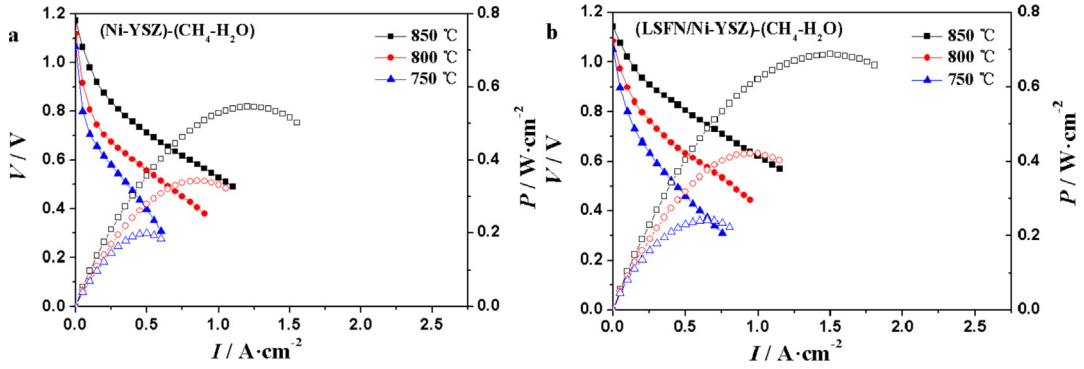

Fig. 4. The I–V (P) curves of a) (Ni–YSZ)–(CH_4–H_2O) and b) (LSFN/Ni–YSZ)–(CH_4–H_2O) from 850 to 750 °C.

severe coking on the Ni-based anode. In contrast, LSFN/Ni–YSZ showed superior stability in each of the two fuels. When fed with CH_4–H_2O and CH_4–air, the catalyst-modified cell was stable for at least 110 h and 120 h, respectively. The improvement in the stability was apparently due to the loading of the catalytic layer on the Ni-based anode, which converted methane into syngas and prevented it from directly contacting the Ni cermet anode. In both the conventional cell and the catalyst-modified cell, the cells using CH_4–air fuel showed better stability than the one using CH_4–H_2O fuel.

3.6. Post-test analyses of cells

After the stability tests in CH_4–H_2O and CH_4–air, the catalyst and anode surfaces were characterized by SEM as shown in Fig. 9 and Fig. 10. Compared with the fresh surfaces (Figs. 9a and 10a), after the stability tests, catalyst and anode particles were obviously aggregated (Fig. 9b&c, Fig. 10b&c). Although coarsening and sintering were observed, its porosities of the anode and catalyst layers were maintained.

EDX analysis was performed for the fresh (Fig. 9d) and aged catalyst surfaces which were exposed to CH_4–H_2O (Fig. 9e) and CH_4–air (Fig. 9f). The average carbon content of a fresh catalyst surface (Fig. 9d) was about 22.67 at.%, which is possibly derived from the pore-formers (glycerol and isopropyl alcohol) in the catalyst layer. After stability tests, the average carbon contents of the catalyst layer using CH_4–H_2O and CH_4–air were about 16.24 at.% and 6.45 at.%. Compared with the fresh catalyst layer

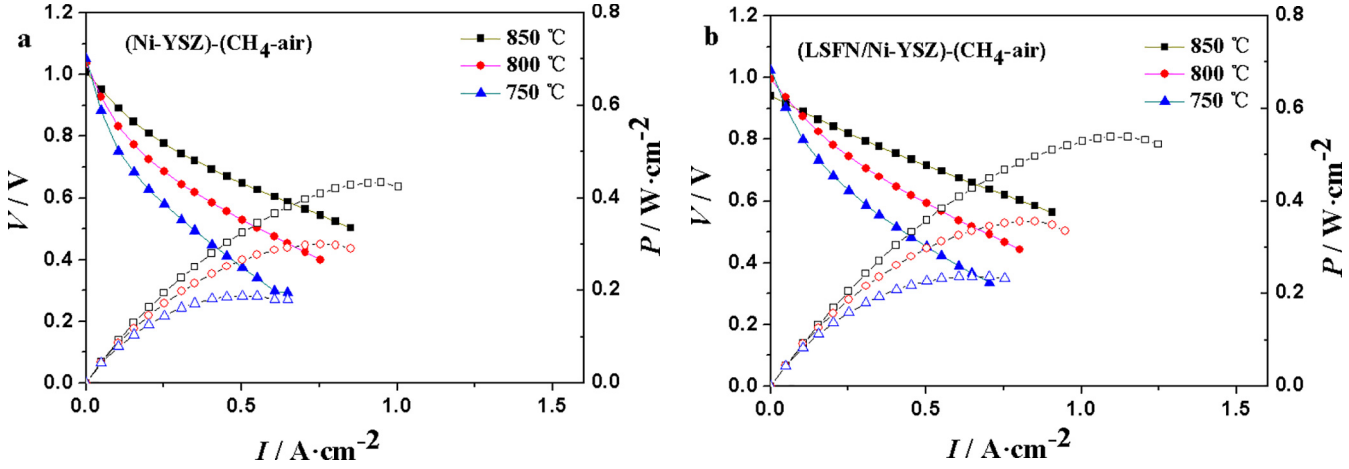

Fig. 5. The I–V (P) curves of a) (Ni–YSZ)–(CH_4–air) and b) (LSFN/Ni–YSZ)–(CH_4–air) from 850 to 750 °C.

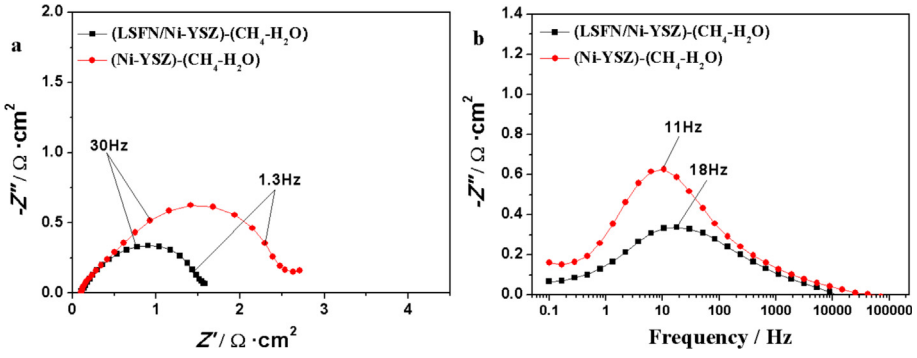

Fig. 6. Comparison on EIS of (LSNF/Ni–YSZ)–(CH_4–H_2O) and (Ni–YSZ)–(CH_4–H_2O) at 850 °C: a) Nyquist plot and b) Bode plot.

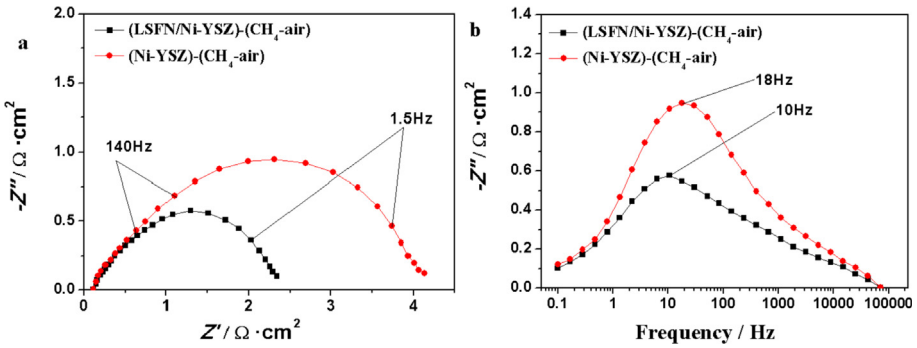

Fig. 7. Comparison on EIS of (LSNF/Ni–YSZ)–(CH_4–air) and (Ni–YSZ)–(CH_4–air) at 850 °C: a) Nyquist plot and b) Bode plot.

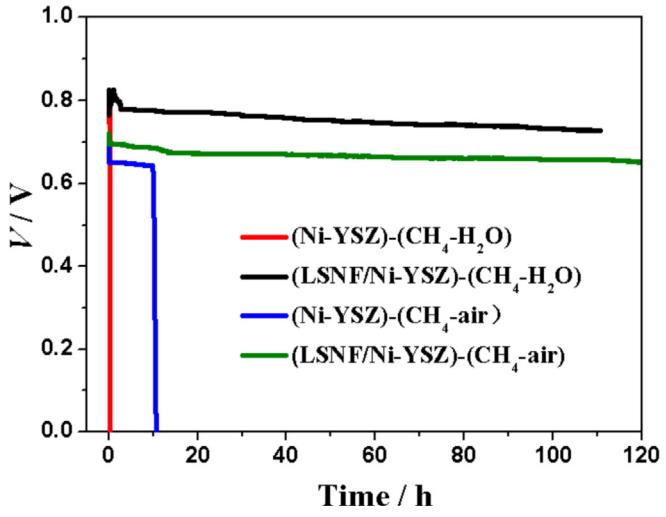

Fig. 8. Durability of Ni–YSZ and LSFN/Ni–YSZ using CH_4–H_2O fuel and CH_4–air fuel at a current of 335 mA cm^{-2} at 800 °C.

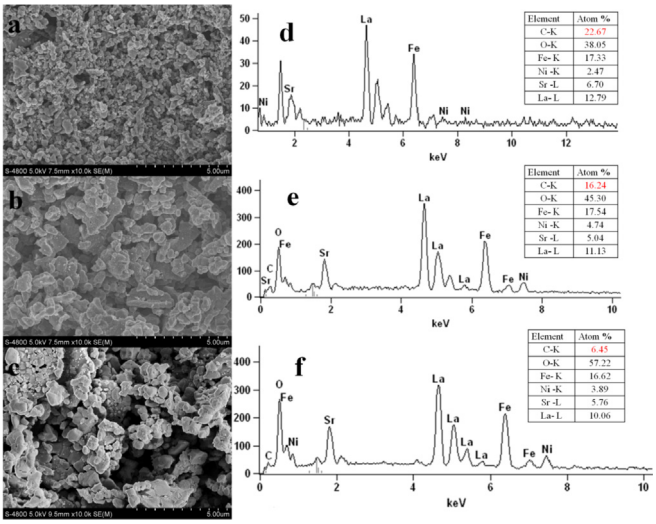

Fig. 9. SEM images and EDX profiles of the catalyst surfaces: a) and d) the fresh H-reduced cell, b) and e) the cell after operation with CH_4–H_2O fuel, c) and f) the cell after operation with CH_4–air fuel under a 335 mA cm^{-2} current at 800 °C.

surface, the low carbon content of the catalyst-modified cells indicated that the Ni–Fe alloy composite catalyst layer effectively prevented coking on the Ni–YSZ anode. For comparison purpose, the fresh (Fig. 10e) H-reduced and aged anode surfaces of a blank cell without the catalyst layer which were exposed to CH_4–H_2O (Fig. 10e) and CH_4–air (Fig. 10f) were also analyzed. The average carbon content of the aged anode surfaces were about 58.37 at. % and 41.89 at. % after operation with CH_4–H_2O fuel and CH_4–air, respectively, which were much higher than that of the fresh anode surface of 19.76 at.%, indicating severe coking without the catalyst layer.

3.7. *Analysis of carbon deposition on the Ni-YSZ anodes fed with CH_4–H_2O/air fuels*

Under using methane-H_2O/air fuels, the amount of carbon deposition on SOFCs depends on the balance between carbon formation and carbon elimination reactions. In this work, the carbon deposition using 97% CH_4–3% H_2O was higher than when 30% CH_4–70% air was used for the following reasons:

(1) For CH_4–H_2O, the methane content was 97%, while it was only 30% for the CH_4–air fuel. The higher methane content led to a higher carbon deposition.
(2) In CH_4–air, the molar ratio of CH_4/O_2 was close to the stoichiometric ratio in the POM reaction of 2:1 (Eq. (4)). The Ni–Fe alloy composite catalyst exhibited a high catalytic activity for the POM reaction to generate syngas, which is less prone to coking. Additionally, increasing amounts of H_2O and CO_2 were generated due to the electrochemical reactions of syngas, which also helped resist carbon deposition (Eqs. (5) and (6)) [47]. The carbon formation reaction from methane cracking simultaneously occurred on the Ni–Fe alloy composite catalyst (Eq. (7)). The produced carbon could be removed because of the fast carbon combustion reaction in Eqs. (8)–(10). For CH_4–H_2O, because of insufficient steam, the cracking and carbon deposition occur in a short time.
(3) From a thermodynamics perspective, the reformation of methane steam (Eq. (6)) is a highly endothermic process that requires a large energy input, while the partial oxidation of methane (Eq. (4)) is an exothermic reaction which releases energy. Therefore, methane steam reforming would reduce the transient temperature at the anode which decreased the cell performance, while the partial oxidation of methane would increase the transient temperature at the anode and further promote a series of reactions. From the perspective of dynamics, the kinetic reaction rate of methane steam reforming is slower than that of the partial methane oxidation, which increased the probability of carbon deposition.

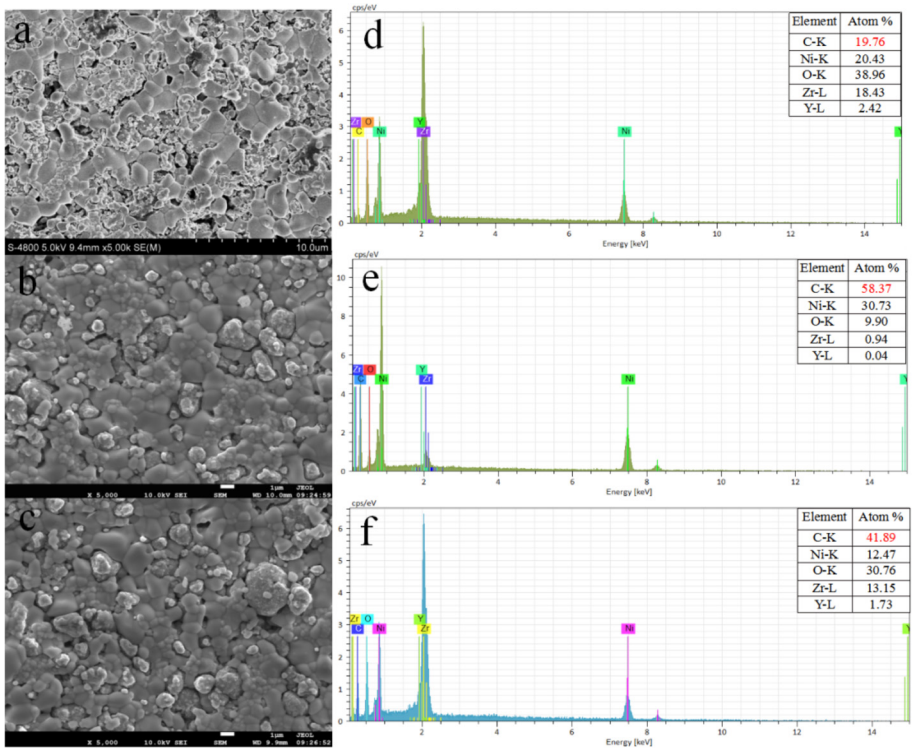

Fig. 10. SEM images and EDX profiles of the anode surface: a) and d) the fresh H-reduced cell, b) and e) the aged cell after operation with CH_4–H_2O fuel, c) and f) the cell after operation with CH_4–air fuel under a 335 mA cm^{-2} current at 800 °C.

$$2CH_4 + O_2 = 2CO + 4H_2 \quad (4)$$

$$CH_4 + CO_2 = 2CO + 2H_2 \quad (5)$$

$$CH_4 + H_2O = CO + 3H_2 \quad (6)$$

$$CH_4 = C + 2H_2 \quad (7)$$

$$C + H_2O = CO + H_2 \quad (8)$$

$$2C + O_2 = 2CO \quad (9)$$

$$C + O_2 = CO_2 \quad (10)$$

4. Conclusion

Due to their good catalytic performance for breaking C–H bonds and high solubility for carbon, Ni-based anodes suffer from carbon deposition when CH_4-based fuels are used. In this work, a Ni–Fe alloy composite catalyst, formed via the *in situ* reduction of perovskite $La_{0.7}Sr_{0.3}Fe_{0.8}Ni_{0.2}O_{3-\delta}$ (LSFN), was directly painted onto a Ni–YSZ anode as a catalyst layer for direct-methane SOFCs. The electrochemical performance and stability of the catalyst-modified cells were investigated and compared with conventional cells. The application of the Ni–Fe alloy composite catalyst layer improved the electrochemical performance and cell stability operated using the CH_4-based fuels. The methane present in the CH_4–H_2O and CH_4–air fuels was partially converted to syngas ($CO + H_2$) by the catalyst layer before it reached the anode. The catalyst-modified cells fed with 30% CH_4–70% air showed better operation stability than those fed with 97% CH_4–3% H_2O due to the fast carbon elimination rate. In summary, the Ni–Fe alloy composite has a promising application for direct-methane SOFCs.

Declaration of competing interest

The authors declared that they have no conflicts of interest to this work.We declare that we do not have any commercial or associative interest that represents a conflict of interest in connection with the work submitted.

CRediT authorship contribution statement

Xiuqing Lv: Conceptualization, Methodology, Investigation, Data curation, Writing - original draft. **Huili Chen:** Resources, Writing - review & editing, Supervision, Data curation. **Wei Zhou:** Resources, Writing - review & editing, Supervision, Data curation. **Fangqin Cheng:** Writing - review & editing. **Si-Dian Li:** Writing - review & editing. **Zongping Shao:** Writing - review & editing.

Acknowledgements

This work was supported by the National Natural Science Foundation of China-Shanxi Coal-based Low Carbon Joint Fund (U1610254); Coal Seam Gas Joint Foundation of Shanxi (2015012016); Shanxi “1331 Project” Engineering Research Center (1331ERC: PT201807); Shanxi Province Science Foundation (2016011025); Shanxi Scholarship Council of China (2016-010) and Shanxi “1331 Project” Key Innovative Research Team (”1331KIRT”).

References

[1] N. Mahato, A. Banerjee, A. Gupta, S. Omar, K. Balani, Progress in material selection for solid oxide fuel cell technology: a review, Prog. Mater. Sci. 72

(2015) 141–337.
[2] F. Ramadhani, M.A. Hussain, H. Mokhlis, S. Hajimolana, Optimization strategies for solid oxide fuel cell (SOFC) application: a literature survey, Renew. Sustain. Energy Rev. 76 (2017) 460–484.
[3] Z. Gao, L.V. Mogni, E.C. Miller, J.G. Railsback, S.A. Barnett, A perspective on low-temperature solid oxide fuel cells, Energy Environ. Sci. 9 (2016) 1602–1644.
[4] D. Chen, C. Chen, Z.M. Baiyee, Z. Shao, F. Ciucci, Nonstoichiometric oxides as low-cost and highly-efficient oxygen reduction/evolution catalysts for low-temperature electrochemical devices, Chem. Rev. 115 (2015) 9869–9921.
[5] Z. Ud Din, Z.A. Zainal, The fate of SOFC anodes under biomass producer gas contaminants, Renew. Sustain. Energy Rev. 72 (2017) 1050–1066.
[6] B. Hua, M. Li, Y.-F. Sun, Y.-Q. Zhang, N. Yan, J. Li, T. Etsell, P. Sarkar, J.-L. Luo, Grafting doped manganite into nickel anode enables efficient and durable energy conversions in biogas solid oxide fuel cells, Appl. Catal. B Environ. 200 (2017) 174–181.
[7] Q. Bkour, K. Zhao, L. Scudiero, D.J. Han, C.W. Yoon, O.G. Marin-Flores, M.G. Norton, S. Ha, Synthesis and performance of ceria-zirconia supported Ni-Mo nanoparticles for partial oxidation of isooctane, Appl. Catal. B Environ. 212 (2017) 97–105.
[8] C. Duan, R.J. Kee, H. Zhu, C. Karakaya, Y. Chen, S. Ricote, A. Jarry, E.J. Crumlin, D. Hook, R. Braun, N.P. Sullivan, R. O'Hayre, Highly durable, coking and sulfur tolerant, fuel-flexible protonic ceramic fuel cells, Nature 557 (2018) 217–222.
[9] D. Pumiglia, S. Vaccaro, A. Masi, S.J. McPhail, M. Falconieri, S. Gagliardi, L. Della Seta, M. Carlini, Aggravated test of Intermediate temperature solid oxide fuel cells fed with tar-contaminated syngas, J. Power Sources 340 (2017) 150–159.
[10] D. Papurello, V. Chiodo, S. Maisano, A. Lanzini, M. Santarelli, Catalytic stability of a Ni-Catalyst towards biogas reforming in the presence of deactivating trace compounds, Renew. Energy 127 (2018) 481–494.
[11] S.Y. Gómez, D. Hotza, Current developments in reversible solid oxide fuel cells, Renew. Sustain. Energy Rev. 61 (2016) 155–174.
[12] D. Lee, J. Myung, J. Tan, S.-H. Hyun, J.T.S. Irvine, J. Kim, J. Moon, Direct methane solid oxide fuel cells based on catalytic partial oxidation enabling complete coking tolerance of Ni-based anodes, J. Power Sources 345 (2017) 30–40.
[13] P. Boldrin, E. Ruiz-Trejo, J. Mermelstein, J.M. Bermudez Menendez, T. Rami Rez Reina, N.P. Brandon, Strategies for carbon and sulfur tolerant solid oxide fuel cell materials, incorporating lessons from heterogeneous catalysis, Chem. Rev. 116 (2016) 13633–13684.
[14] S. Sengodan, R. Lan, J. Humphreys, D. Du, W. Xu, H. Wang, S. Tao, Advances in reforming and partial oxidation of hydrocarbons for hydrogen production and fuel cell applications, Renew. Sustain. Energy Rev. 82 (2018) 761–780.
[15] W. Wang, C. Su, Y. Wu, R. Ran, Z. Shao, Progress in solid oxide fuel cells with nickel-based anodes operating on methane and related fuels, Chem. Rev. 113 (2013) 8104–8151.
[16] S.P.S. Shaikh, A. Muchtar, M.R. Somalu, A review on the selection of anode materials for solid-oxide fuel cells, Renew. Sustain. Energy Rev. 51 (2015) 1–8.
[17] H. Ding, Z. Tao, S. Liu, Y. Yang, A redox-stable direct-methane solid oxide fuel cell (SOFC) with $Sr_2FeNb_{0.2}Mo_{0.8}O_{6-\delta}$ double perovskite as anode material, J. Power Sources 327 (2016) 573–579.
[18] M. Miyake, M. Iwami, M. Takeuchi, S. Nishimoto, Y. Kameshima, Electrochemical performance of $Ni_{0.8}Cu_{0.2}/Ce_{0.8}Gd_{0.2}O_{1.9}$ cermet anodes with functionally graded structures for intermediate-temperature solid oxide fuel cell fueled with syngas, J. Power Sources 390 (2018) 181–185.
[19] B. Han, K. Zhao, X. Hou, D.-J. Kim, B.-H. Kim, S. Ha, M.G. Norton, Q. Xu, B.-G. Ahn, Ni-$(Ce_{0.8-x}Ti_x)Sm_{0.2}O_{2-\delta}$ anode for low temperature solid oxide fuel cells running on dry methane fuel, J. Power Sources 338 (2017) 1–8.
[20] T. Wan, A. Zhu, Y. Guo, C. Wang, S. Huang, H. Chen, G. Yang, W. Wang, Z. Shao, Co-generation of electricity and syngas on proton-conducting solid oxide fuel cell with a perovskite layer as a precursor of a highly efficient reforming catalyst, J. Power Sources 348 (2017) 9–15.
[21] J. Zhao, X. Xu, M. Li, W. Zhou, S. Liu, Z. Zhu, Coking-resistant $Ce_{0.8}Ni_{0.2}O_{2-\delta}$internal reforming layer for direct methane solid oxide fuel cells, Electrochim. Acta 282 (2018) 402–408.
[22] W. Wang, R. Ran, Z. Shao, Lithium and lanthanum promoted Ni-Al_2O_3 as an active and highly coking resistant catalyst layer for solid-oxide fuel cells operating on methane, J. Power Sources 196 (2011) 90–97.
[23] J. Zhao, X. Xu, W. Zhou, Z. Zhu, An in situ formed MnO–Co composite catalyst layer over Ni–$Ce_{0.8}Sm_{0.2}O_{2-\delta}$ anodes for direct methane solid oxide fuel cells, J. Mater. Chem. A 5 (2017) 6494–6503.
[24] L. Bian, C. Duan, L. Wang, R. O'Hayre, J. Cheng, K.-C. Chou, Ce-doped $La_{0.7}Sr_{0.3}Fe_{0.9}Ni_{0.1}O_{3-\delta}$ as symmetrical electrodes for high performance direct hydrocarbon solid oxide fuel cells, J. Mater. Chem. A 5 (2017) 15253–15259.
[25] Y.F. Sun, J.H. Li, L. Cui, B. Hua, S.H. Cui, J. Li, J.L. Luo, A-site-deficiency facilitated in situ growth of bimetallic Ni-Fe nano-alloys: a novel coking-tolerant fuel cell anode catalyst, Nanoscale 7 (2015) 11173–11181.
[26] Q. Yang, J. Chen, C. Sun, L. Chen, Direct operation of methane fueled solid oxide fuel cells with Ni cermet anode via Sn modification, Int. J. Hydrogen Energy 41 (2016) 11391–11398.
[27] B. Farrell, S. Linic, Direct electrochemical oxidation of ethanol on SOFCs: improved carbon tolerance of Ni anode by alloying, Appl. Catal. B Environ. 183 (2016) 386–393.
[28] G. Ding, T. Gan, J. Yu, P. Li, X. Yao, N. Hou, L. Fan, Y. Zhao, Y. Li, Carbon-resistant $Ni_{1-x}Co_x$-$Ce_{0.8}Sm_{0.2}O_{1.9}$ anode for solid oxide fuel cells fed with methanol, Catal. Today 298 (2017) 250–257.
[29] K. Zhao, X. Hou, Q. Bkour, M.G. Norton, S. Ha, NiMo-ceria-zirconia catalytic reforming layer for solid oxide fuel cells running on a gasoline surrogate, Appl. Catal. B Environ. 224 (2018) 500–507.
[30] K. Li, L. Jia, X. Wang, J. Pu, B. Chi, L. Jian, Methane on-cell reforming in nickel–iron alloy supported solid oxide fuel cells, J. Power Sources 284 (2015) 446–451.
[31] Y.M. Park, H. Kim, An additional layer in an anode support for internal reforming of methane for solid oxide fuel cells, Int. J. Hydrogen Energy 39 (2014) 16513–16523.
[32] X. Kong, Y. Tian, X. Zhou, X. Wu, J. Zhang, Surface tuned $La_{0.9}Ca_{0.1}Fe_{0.9}Nb_{0.1}O_{3-\delta}$ based anode for direct methane solid oxide fuel cells by infiltration method, Electrochim. Acta 234 (2017) 71–81.
[33] D. Ding, X. Li, S.Y. Lai, K. Gerdes, M. Liu, Enhancing SOFC cathode performance by surface modification through infiltration, Energy Environ. Sci. 7 (2014) 552.
[34] T. Pussacq, O. Mentré, F. Tessier, A. LÖfberg, M. Huvé, J.G. Caballer, S. Colis, H. Kabbour, Nanometric nickel exsolution in the hexagonal perovskite $Ba_8Ta_6NiO_{24}$: survey of the structural, magnetic and catalytic features, J. Alloy. Comp. 766 (2018) 987–993.
[35] S. Sengodan, Y.-W. Ju, O. Kwon, A. Jun, H.Y. Jeong, T. Ishihara, J. Shin, G. Kim, Self-decorated MnO nanoparticles on double perovskite solid oxide fuel cell anode by in situ exsolution, ACS Sustain. Chem. Eng. 5 (2017) 9207–9213.
[36] Z. Du, H. Zhao, S. Yi, Q. Xia, Y. Gong, Y. Zhang, X. Cheng, Y. Li, L. Gu, K. Swierczek, High-performance anode material $Sr_2FeMo_{0.65}Ni_{0.35}O_{6-\delta}$ with in situ exsolved nanoparticle catalyst, ACS Nano 10 (2016) 8660–8669.
[37] X. Chen, W. Ni, J. Wang, Q. Zhong, M. Han, T. Zhu, Exploration of Co-Fe alloy precipitation and electrochemical behavior hysteresis using Lanthanum and Cobalt co-substituted $SrFeO_{3-\delta}$ SOFC anode, Electrochim. Acta 277 (2018) 226–234.
[38] J. Li, Y. Yu, Y.-M. Yin, N. Zhou, Z.-F. Ma, A novel high performance composite anode with in situ growth of Fe-Ni alloy nanoparticles for intermediate solid oxide fuel cells, Electrochim. Acta 235 (2017) 317–322.
[39] K.-Y. Lai, A. Manthiram, Self-regenerating Co–Fe nanoparticles on perovskite oxides as a hydrocarbon fuel oxidation catalyst in solid oxide fuel cells, Chem. Mater. 30 (2018) 2515–2525.
[40] H. Chang, H. Chen, Z. Shao, J. Shi, J. Bai, S.-D. Li, In situ fabrication of (Sr,La)FeO_4 with CoFe alloy nanoparticles as an independent catalyst layer for direct methane-based solid oxide fuel cells with a nickel cermet anode, J. Mater. Chem. A 4 (2016) 13997–14007.
[41] Z. Wang, Y.-M. Yin, Y. Yu, Y. Song, Z.-F. Ma, J. Yin, Roles of Fe Ni nanoparticles and $SrLaFeO_4$ substrate in the performance and reliability of a composite anode prepared through in-situ exsolution for intermediate temperature solid oxide fuel cells (I), Int. J. Hydrogen Energy 43 (2018) 10440–10447.
[42] L. Xu, Y.-M. Yin, N. Zhou, Z. Wang, Z.-F. Ma, Sulfur tolerant redox stable layered perovskite $SrLaFeO_{4-\delta}$ as anode for solid oxide fuel cells, Electrochem. Commun. 76 (2017) 51–54.
[43] H. Zhu, W. Wang, R. Ran, Z. Shao, A new nickel–ceria composite for direct-methane solid oxide fuel cells, Int. J. Hydrogen Energy 38 (2013) 3741–3749.
[44] D.A. Hickman, L.D. Schmidt, Production of syngas by direct catalytic oxidation of methane, Science 259 (1993) 343–346.
[45] A.T. Ashcroft, A.K. Cheetham, J.S. Foord, M.L.H. Green, C.P. Grey, A.J. Murrell, P.D.F. Vernon, Selective oxidation of methane to synthesis gas using transition metal catalysts, Nature 344 (1990) 319–321.
[46] T.F. Guiberti a, C. Garnier a, P. Scouflaire, J. Caudal, B. Labegorre, T. Schuller, N. Darabiha, Experimental and numerical analysis of noncatalytic partial oxidation and steam reforming of $CH_4/O_2/N_2/H_2O$ mixtures including the impact of radiative heat losses, Int. J. Hydrogen Energy 41 (2016) 8616–8626.
[47] H. Chen, Y. Wu, G. Yang, J. Shi, W. Zhou, J. Bai, S. Li, Z. Shao, Direct power generation from low concentration coal-bed-gas by a catalyst-modified solid oxide fuel cell, ChemElectroChem 5 (2018) 1459–1466.